Room-temperature spin filtering in a $CoFe_2O_4/MgAl_2O_4/Fe_3O_4$ magnetic tunnel barrier

Michael G. Chapline[1] and Shan X. Wang[1,2]
[1]*Department of Materials Science and Engineering Stanford University, Stanford, California 94305, USA*
[2]*Department of Electrical Engineering, Stanford University, Stanford, California 94305, USA*
(Received 20 December 2005; revised manuscript received 17 April 2006; published 17 July 2006)

By growing ultrathin and high quality $CoFe_2O_4/MgAl_2O_4/Fe_3O_4$ epitaxial multilayers, we have demonstrated a room temperature spin filter junction, which could open the way for highly polarized spin injection, single-qubit spintronic measurements, magnetic field sensing, and other applications. In these devices the Fe_3O_4 layer functions as a source of spin polarized electrons while the $CoFe_2O_4/MgAl_2O_4$ double barrier functions as a spin filter. The current-voltage curves depend on the relative orientation of the magnetization of the Fe_3O_4 and $CoFe_2O_4$ layers and display a large magnetoresistive effect. The inferred net spin polarizations produced by the junctions typically exceeded 70%.

DOI: 10.1103/PhysRevB.74.014418 PACS number(s): 75.70.Cn, 85.75.−d, 85.70.Ge, 73.40.Gk

I. INTRODUCTION

Spintronics is a new field of electronics based upon manipulating the spin of the electron. Devices based on spintronics are attractive both because of the possibilities inherent in the quantum nature of single spins and the relatively small amount of energy required to manipulate spins. Of course, an essential prerequisite to realizing spintronics devices are methods for generating and detecting polarized spins. Efficient spin injection into semiconductors is still a challenge with only partial success achieved to date, particularly at room temperature.[1] One promising approach to spin injection is to use a spin filter tunnel barrier that favors one spin polarization over the other. It has also been proposed that a spin filter tunnel barrier in conjunction with a single electron quantum dot may be used to measure the spin of a single electron.[2] Spin filters could also be used to measure small variations in magnetic fields. For example, Worledge and Geballe[3] have proposed fabricating a double spin filter junction that is expected to be several orders of magnitude more sensitive than magnetic tunnel junctions. Unfortunately, spin filter tunnel barriers have only been demonstrated at low temperatures, which for many applications limit the practical usefulness of such devices.

Spin filtering was first demonstrated by studying the spin polarization of field emission from EuS coated *W* tips.[4–6] EuS is a ferromagnetic semiconductor with a Curie temperature (T_C) of 16.8 K. Due to exchange interactions between conduction electrons and magnetically ordered Eu ions, there is an energy splitting of the conduction band creating different barrier heights for spin up and spin down electrons. The preferential filtering is due to the exponential dependence of the tunneling process on the barrier height. As a result, one spin channel will have a much larger tunneling probability with nearly 90% spin-polarized current having been achieved. However, for temperatures above T_C there is no longer an exchange splitting and both spin up and spin down electrons will experience the same barrier.

$CoFe_2O_4$ is a promising material for use as a spin filter because it is both insulating and has a T_C well above room temperature. We have demonstrated that $CoFe_2O_4$ can indeed be used as a room temperature spin filter by fabricating $Au/CoFe_2O_4/MgAl_2O_4/Fe_3O_4$ junctions. Gajek *et al.*[7] used a similar architecture to demonstrate a low temperature spin filter effect in $BiMnO_3$ tunnel barriers by fabricating $Au/BiMnO_3/SrTiO_3/La_{2/3}Sr_{1/3}MnO_3$ junctions. Figure 1 illustrates our approach. In these devices the Fe_3O_4 layer serves as a source of spin polarized electrons while the $CoFe_2O_4/MgAl_2O_4$ double barrier functions as the spin filter. The $MgAl_2O_4$ layer is used to decouple the $CoFe_2O_4$ and Fe_3O_4 and allows the magnetizations of the layers to be independently switched. The evidence for spin filtering is provided by the dependence of the tunneling current versus voltage (I-V) curve on the relative orientation of the magnetizations of the Fe_3O_4 and $CoFe_2O_4$ layers.

II. EXPERIMENTAL

The $CoFe_2O_4/MgAl_2O_4/Fe_3O_4$ films and underlying $CoCr_2O_4$ buffer layer were grown on (001) $MgAl_2O_4$ oriented substrates by pulsed laser deposition (PLD). A focused KrF excimer laser (248 nm) with a repetition rate of 10 Hz and a fluence of ~ 3 J/cm^2 at the target was used. The $CoCr_2O_4$ buffer layer was grown at a temperature of 650 °C in a 10 mTorr O_2 atmosphere. A typical deposition rate for the $CoCr_2O_4$ layer was 2 nm/min. The Fe_3O_4 layer was deposited at 350 °C under 10^{-6} Torr O_2 atmosphere while the $CoFe_2O_4$ and $MgAl_2O_4$ layers were deposited in a 10^{-5} Torr O_2 atmosphere at 350 °C. A typical deposition rate for the $MgAl_2O_4$, $CoFe_2O_4$, and Fe_3O_4 films was 0.6 nm/min. $Au/CoFe_2O_4/MgAl_2O_4/Fe_3O_4$ junctions were fabricated by depositing 25 μm$\times$25 μm Au pads using electron beam evaporation through a shadow mask.

We were able to quickly characterize the electrical properties of our films and devices by making use of a conductive atomic force microscope (CAFM). For these measurements the CAFM tip was held fixed at a particular point and in contact with the surface as an I-V curve was recorded. The deflection of the cantilever was measured and did not change during the I-V scan which indicates that the contact between the tip and the surface was stable. A small electromagnet was added to the AFM stage capable of applying fields up to 600 Oe in the plane of the film.

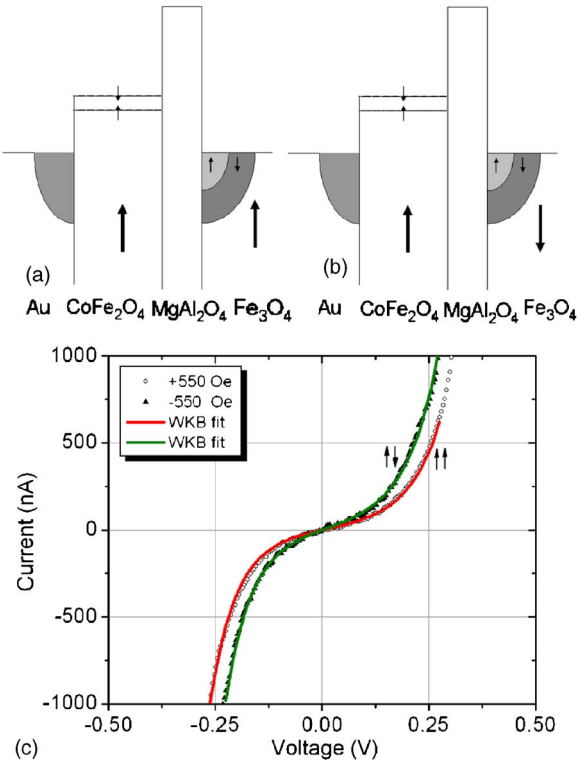

FIG. 1. (Color online) Schematic illustration of spin filtering in our tunnel junction. The $MgAl_2O_4$ layer is used to decouple the $CoFe_2O_4$ and Fe_3O_4 and allows the magnetizations of the layers to be independently switched. (a) When the magnetizations of the $CoFe_2O_4$ and Fe_3O_4 layers are parallel, the majority (spin up) electrons in the Fe_3O_4 layer are able to preferentially tunnel through the $CoFe_2O_4/MgAl_2O_4$ bilayer due to the lower barrier height for majority electrons in the $CoFe_2O_4$ layer. (b) When the magnetizations of the $CoFe_2O_4$ and Fe_3O_4 layers are antiparallel, the minority spin electrons in the Fe_3O_4 layer are able to preferentially tunnel through the $CoFe_2O_4/MgAl_2O_4$ bilayer. Because the electrons at the Fermi surface in the Fe_3O_4 layer are predominately minority spin electrons, the tunneling current will be largest when the magnetizations of the $CoFe_2O_4$ and Fe_3O_4 layers are antiparallel. (c) I-V curves for an $Au/CoFe_2O_4(3\ nm)/MgAl_2O_4(1\ nm)/Fe_3O_4$ (30 nm) sample when the magnetizations of the $CoFe_2O_4$ and Fe_3O_4 layers are parallel and antiparallel, measured using a CAFM tip held against the Au pad. Solid lines are the fits of the two I-V curves using our WKB approximation Eq. (1).

III. RESULTS

The Verwey transition in thin films of Fe_3O_4 is a useful gauge for determining the quality of the films.[8] The transition was clearly visible for films as thin as 20 nm, which suggests our Fe_3O_4 films have near perfect stoichiometry and are of high quality. The $CoFe_2O_4$ and $MgAl_2O_4$ layers were grown under conditions that did not oxidize the Fe_3O_4 surface.[9] This was confirmed by x-ray photoelectron spectroscopy (XPS) and observation of the Verwey transition. XPS was also used to determine the composition of the $CoFe_2O_4$ layer by comparing the (Fe 2p/Co 2p) transitions in the films with bulk Co ferrite samples. The ratio of the Fe to Co is very close to two, indicating the films have near perfect stoichiometry. The spectra also indicate the Co ions are in the +2 formal oxidation state and nearly all of the Fe ions are in the +3 formal oxidation state.

In order to observe the spin filter effect it must be possible to independently switch the magnetization of the Fe_3O_4 and $CoFe_2O_4$ layers. Previous studies of $CoFe_2O_4/Fe_3O_4$ bilayers indicated that the layers are strongly magnetically coupled.[10] In the current study we were able to reduce their magnetic coupling by inserting a thin film of $MgAl_2O_4$ between the $CoFe_2O_4$ and Fe_3O_4 layers. Figure 2 shows the magnetic properties for $CoFe_2O_4(3\ nm)/MgAl_2O_4(1\ nm)/Fe_3O_4(25\ nm)$, and $MgAl_2O_4(3\ nm)/Fe_3O_4$ (25 nm) samples. The contribution from the $CoFe_2O_4$ layer can be clearly seen by comparing the two figures. The ratio of the contribution of the Fe_3O_4 and $CoFe_2O_4$ layers to the saturation magnetization corresponds to the expected value based upon the magnetic moments from the two layers. Figure 2(b) also shows a minor loop where the field is ramped from +10 kOe to −800 Oe and back to +10 kOe. This minor loop shows it is possible to switch the magnetization of the Fe_3O_4 layer without affecting the $CoFe_2O_4$ layer. The offset of the minor loop can be used to measure the magnetic coupling of the $CoFe_2O_4$ and Fe_3O_4 layers. The minor loops for samples fabricated with a 1 nm $MgAl_2O_4$ spacer were typically offset by 4–8 Oe. This small offset is most likely the result of small ferromagnetic "orange peel" coupling due to correlated surface variations.[11] The insert in Fig. 2(b) shows the complete hysteresis loop. A sharp step is not visible since the magnetization loop from the $CoFe_2O_4$ is not very square.

By measuring the local tunneling current on $CoFe_2O_4$ $(3\ nm)/Fe_3O_4(30\ nm)$ and $MgAl_2O_4(3\ nm)/Fe_3O_4$ (30 nm) samples with the CAFM tip in contact with the surface of the oxide we were able to determine the intrinsic electrical properties of both $MgAl_2O_4$ and $CoFe_2O_4$ free from pinholes. We have previously reported the electrical properties of $CoFe_2O_4/Fe_3O_4$ bilayers.[12] From fitting the measured tunneling data to Simmons' formula for the tunneling current through an insulating barrier,[13] we obtained a barrier height of 0.29 eV for the $CoFe_2O_4$ layer. Figure 3(a) shows a typical CAFM I-V curve for a $MgAl_2O_4$ $(3\ nm)/Fe_3O_4$ (30 nm) bilayer. The I-V curve was measured at multiple locations on several different samples and always yielded a barrier height of approximately 0.8 eV. The fitted barrier thickness of the $MgAl_2O_4$ layer and effective tunneling area agreed well with the estimates.

By using the CAFM to measure local I-V curves for $CoFe_2O_4/MgAl_2O_4/Fe_3O_4$ samples with the tip directly in contact with the surface of the $CoFe_2O_4$ layer we were able to determine the intrinsic electrical properties of the $CoFe_2O_4/MgAl_2O_4$ double barrier. Simmons' formula, which treats the insulating barrier as a single layer cannot be used when the barrier consists of two layers with very different barrier heights. We have derived a generalization of the Simmons' formula for multilayer barriers by retaining Simmons' semiclassical treatment of the tunneling current as a product of the classical flux of electrons in the electrode hitting the barrier and the quantum mechanical tunneling probability. However, instead of using the average barrier

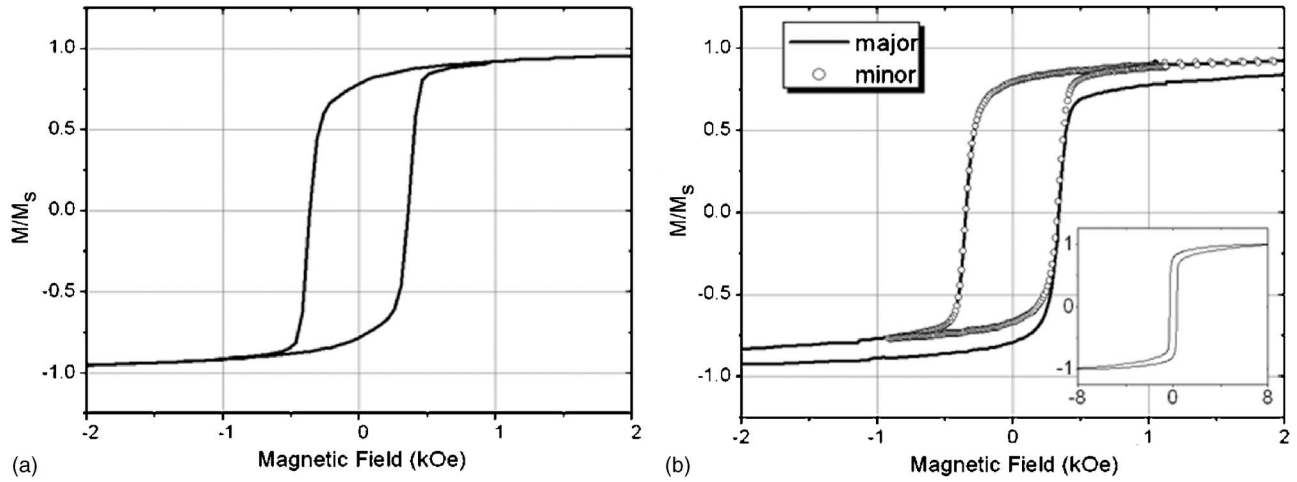

FIG. 2. Magnetization hysteresis loops for (a) $MgAl_2O_4$(3 nm)/Fe_3O_4(25 nm) and (b) $CoFe_2O_4$(3 nm)/$MgAl_2O_4$(1 nm)/Fe_3O_4(25 nm) samples. Solid line represents the major loop while the circles represent the minor loop.

height to evaluate the tunneling probability as Simmons did, we evaluated the tunneling probability as the product of the exact WKB tunneling probabilities for each layer. The details are given in the Appendix. Our expression for the tunneling current density through a bilayer barrier at low voltage bias ($eV < \Phi_1, \Phi_2$) is

$$J = \tilde{J}_0 \frac{(eV)^2}{4} \Bigg\{ [\varepsilon_1(\Phi_1^{1/2} - (\Phi_1 - eV_1)^{1/2}) + \varepsilon_2((\Phi_2 - eV_1)^{1/2} - (\Phi_2 - eV)^{1/2})]^{-2} \times \exp\left(- \frac{2\tilde{A}}{3eV} [\varepsilon_1(\Phi_1^{3/2} - (\Phi_1 - eV_1)^{3/2}) + \varepsilon_2((\Phi_2 - eV_1)^{3/2} - (\Phi_2 - eV)^{3/2})] \right) - [\varepsilon_1((\Phi_1 + eV)^{1/2} - (\Phi_1 + eV_2)^{1/2}) + \varepsilon_2((\Phi_2 + eV_2)^{1/2} - (\Phi_2)^{1/2})]^{-2} \exp\left(- \frac{2\tilde{A}}{3eV} [\varepsilon_1((\Phi_1 + eV)^{3/2} + (\Phi_1 + eV_2)^{3/2}) + \varepsilon_2((\Phi_2 + eV_2)^{3/2} - (\Phi_2)^{3/2})] \right) \Bigg\} \quad (1)$$

where $\tilde{J}_0 = \frac{e}{2\pi^2\hbar}\left(\frac{\Delta x_1}{\varepsilon_1} + \frac{\Delta x_2}{\varepsilon_2}\right)^{-2}$, $\tilde{A} = \frac{2\sqrt{2m}}{\hbar}\left(\frac{\Delta x_1}{\varepsilon_1} + \frac{\Delta x_2}{\varepsilon_2}\right)$, $V_1 = V\frac{\Delta x_1}{\varepsilon_1}\left(\frac{\Delta x_1}{\varepsilon_1} + \frac{\Delta x_2}{\varepsilon_2}\right)^{-1}$, and $V_2 = V\frac{\Delta x_2}{\varepsilon_2}\left(\frac{\Delta x_1}{\varepsilon_1} + \frac{\Delta x_2}{\varepsilon_2}\right)^{-1}$, Δx_1 and Δx_2 are the thicknesses of the two layers, ε_1 and ε_2 are the dielectric constants in the two layers, and Φ_1 and Φ_2 are the two barrier heights. Biases larger than the smallest barrier height will cause the effective width of the barrier to decrease. The above equation does not take this into account and can only be applied when $eV < \Phi_1$, Φ_2. A typical measured I-V curve for a $CoFe_2O_4$(3 nm)/$MgAl_2O_4$(1 nm)/Fe_3O_4(30 nm) sample and WKB fit is shown in Fig. 3(b). Fitting the measured curve to Eq. (1) yielded barrier heights for the $CoFe_2O_4$ and $MgAl_2O_4$ layers that were consistent with the barrier heights obtained from fitting the single layer I-V curves with Simmons' formula.

Magnetic field dependent measurements of the tunneling current were made on Au(50 nm)/$CoFe_2O_4$(1 nm)/$MgAl_2O_4$(3 nm)/Fe_3O_4(30 nm) junctions with the CAFM tip held in contact with the Au pad. Similar measurements using a CAFM have previously been applied to characterize magnetic tunnel junctions.[14] The samples were initially magnetized in a 12 kOe external field before being transferred to the AFM stage. Figure 4 shows a typical plot of the magnetoresistance $[(R - R_{-550\ \mathrm{Oe}})/R_{-550\ \mathrm{Oe}}]$ versus field. The magnetoresistance curve shows a hysteretic behavior with a sharp change corresponding to the switching field of the Fe_3O_4 layer. Repeated measurements on all Au/$CoFe_2O_4$/$MgAl_2O_4$/Fe_3O_4 samples were very reproducible and showed similar results. The saturation magnetostriction strains λ_s for $CoFe_2O_4$ and Fe_3O_4 are 100×10^{-6} and 40×10^{-6}, respectively. Therefore, the change in thickness of the Fe_3O_4 and $CoFe_2O_4$ layers in our samples is so small that magnetostriction effects can be ruled out as an explanation for our observations. In fact, the Fe_3O_4 layer thickness is the same whether its magnetization points to the left or right. In addition, I-V measurements made on Au(50 nm)/$MgAl_2O_4$(3 nm)/Fe_3O_4(30 nm) junctions showed no change in junction resistance with the applied magnetic field.

Figure 1 compares the I-V curves for a 550 Oe field applied parallel and antiparallel to the initial magnetization for another Au/$CoFe_2O_4$/$MgAl_2O_4$/Fe_3O_4 junction. The I-V

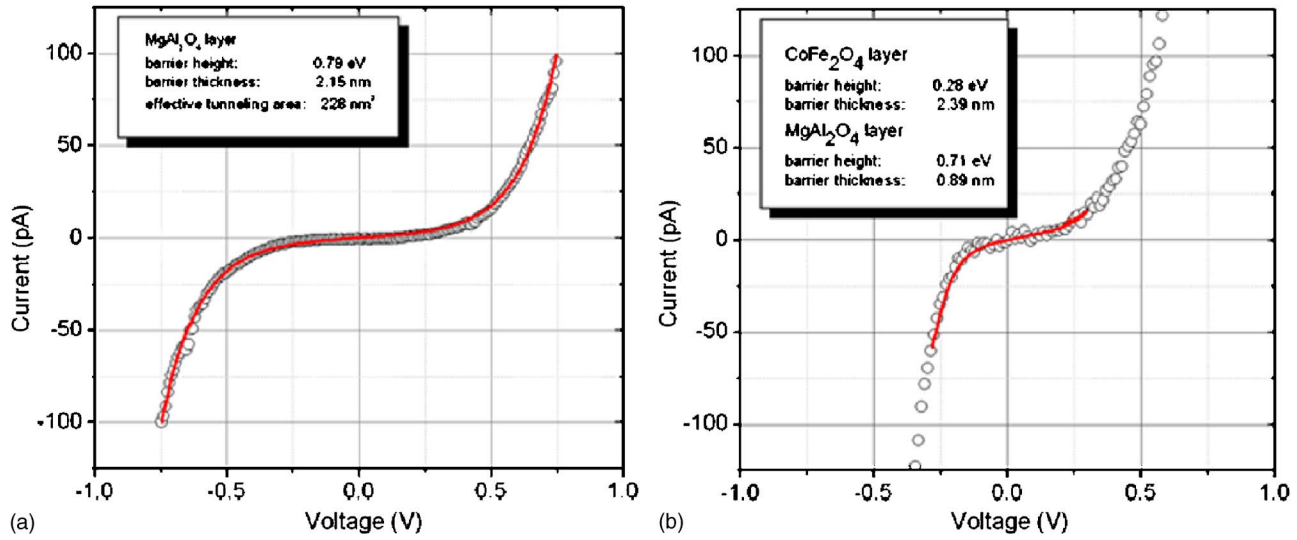

FIG. 3. (Color online) (a) I-V curve for of $MgAl_2O_4$(3 nm)/Fe_3O_4(30 nm) bilayer measured using CAFM with its tip in direct contact with $MgAl_2O_4$. Solid line is fit to Simmons' formula which is valid for biases less than the barrier height. (b) I-V curve for $CoFe_2O_4$(3 nm)/$MgAl_2O_4$(1 nm)/Fe_3O_4(30 nm) measured using CAFM with its tip in direct contact with $CoFe_2O_4$. Solid line is a fit to Eq. (1) which is only valid for biases less than the smallest barrier height.

curves were fitted by assuming that the tunneling current is a sum of two spin-polarized currents. In particular, we assumed that when the magnetizations of the two layers are parallel a fraction f of the tunneling electrons will experience a barrier height $\Phi_\uparrow$ in the $CoFe_2O_4$ layer while a fraction (1-f) will experience a barrier height $\Phi_\downarrow$ in the $CoFe_2O_4$ layer. When the magnetizations of the two layers are antiparallel, a fraction (1-f) will experience a barrier height $\Phi_\uparrow$ while f will experience a barrier height $\Phi_\downarrow$. Values for the barrier thicknesses, the barrier heights for spin up and spin down electrons, and the fraction f of tunneling electrons with spin up were obtained by simultaneously fitting the measured I-V curves when the magnetizations of the $CoFe_2O_4$ and Fe_3O_4 layers are parallel and antiparallel and are shown in Table I. The tunneling area was assumed to be the area of the Au pad and the dielectric constants of the films were assumed to be equal to their bulk values. The difference between the two curves as a function of voltage is determined by the spin polarization of the electrons from the Fe_3O_4 layer and spin splitting of the barrier height in the $CoFe_2O_4$ layer. In all cases the fits give a splitting between the spin up and spin down barriers in the range 0.07–0.12 eV. The net spin polarization of electrons emitted from our tunnel junctions, $(J_\uparrow - J_\downarrow)/(J_\uparrow + J_\downarrow)$, can be calculated from the spin up $J_\uparrow$ and spin down $J_\downarrow$ currents inferred from our fits. The values we calculate for the emitted spin polarization at zero voltage bias when the magnetizations are antiparallel are listed in Table I.

IV. THEORETICAL INTERPRETATION

$CoFe_2O_4$ is traditionally described as having an inverse spinel structure where the O^{2-} ions form an FCC lattice, the tetrahedral (A) sites are occupied by Fe^{3+} ions, and the octahedral (B) sites are occupied by a mixture of Co^{2+} and the Fe^{3+} ions. Correlated electron band theory[15] predicts an insulating gap of 0.63 eV, corresponding to the energy difference between the spin down t_{2g} state for Co^{2+} ions on B-sites and the bottom of the spin down t_{2g} conduction band for Fe^{3+} ions on B-sites. Spin resolved photoemission studies of Fe_3O_4 thin films[16] as well as measurements from $Fe_3O_4/CoCr_2O_4/La_{0.7}Sr_{0.3}MnO_3$ junctions[17] have shown that the conduction electrons provided by the Fe_3O_4 layer have a negative spin polarization. This would have implied that the tunneling current would have been maximal when the magnetizations of the $CoFe_2O_4$ and Fe_3O_4 layers were aligned and it is contrary to what we have observed.

However, several experimental studies[18–20] of single crystals and PLD grown films have indicated that $CoFe_2O_4$ has a partial inverse structure with ~7–20% of the Co^{2+} ions in

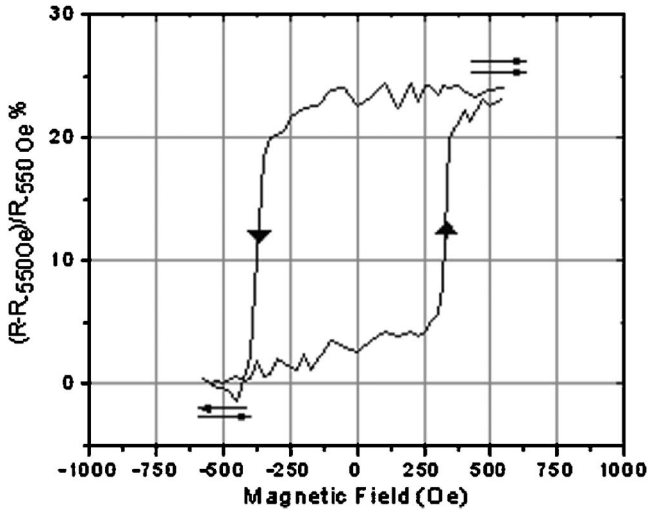

FIG. 4. dI/dV versus applied magnetic field at zero bias voltage for an Au/$CoFe_2O_4$(3 nm)/$MgAl_2O_4$(1 nm)/Fe_3O_4(30 nm) junction measured using CAFM.

TABLE I. Physical parameters extracted from the spin filter junctions.

Sample	I	II			III	IV
$CoFe_2O_4$ layer						
$\Phi_\uparrow$: (eV)	0.3369±.0002	0.3166±.0006	0.3218±.0001	0.2896±.0004	0.3205±.0002	0.3313±.0003
$\Phi_\downarrow$: (eV)	0.3982±.0046	0.4258±.0021	0.4186±.0035	0.4020±.0072	0.4058±.0023	0.4260±.0050
Barrier thickness: (nm)	1.98	2.17	2.45	2.13	2.55	2.48
$MgAl_2O_4$ layer						
Φ: (eV)	0.9747	0.6425	0.7038	0.6902	0.7786	0.7540
Barrier thickness: (nm)	0.92	1.12	0.79	0.81	0.77	0.8
Fraction of electrons from Fe_3O_4 layer with positive spin:	0.3698±.0003	0.3775±.0002	0.3517±.0001	0.3246±.0001	0.4318±.0001	0.4478±.0005
Inferred Fe_3O_4 spin polarization (%):	26	24	30	36	14	10
MR effect near zero bias (%):	26	43	55	75	24	16
Calculated spin polarization emitted from junction when the magnetizations are anti-parallel (%):	64	83	84	87	76	74

tetrahedral *A* sites. The saturation magnetization we measured for 30 nm thick $CoFe_2O_4$ films was ~400 emu/cm^3 Co^{2+} which corresponds to ~10% of the Co^{2+} ions on *A* sites. If the Co^{2+} ions reside on *A* sites, correlated band theory predicts[15] that the highest energy occupied 3*d* state for the Co^{2+} ions on the *A* sites is a spin up e_g state which is shifted downward in energy from the spin down t_{2g} state for Co^{2+} ions on B-sites as indicated in Fig. 5. This prediction is in agreement with magnetic circular dichronism (XMCD) experiments on $CoFe_2O_4$ (Ref. 21), which show a feature in the *M*-shell spectrum associated with the 3*d* e_g state for Co^{2+} ions on *A* sites that is lower in energy than the feature associated with the 3*d* t_{2g} state for the Co^{2+} ions on *B*-sites by 1.5 eV. The t_{2g} state for Co^{2+} ions on *A* sites will be shifted upward in energy from the e_g state by the crystal field splitting at tetrahedral sites. Measurements of the optical reflectance of polarized light from $CoFe_2O_4$ films suggest that the crystal field splitting of these states is 2 eV (Ref. 22). These results suggest that the lowest energy conduction state in $CoFe_2O_4$ will in fact be the spin up 3*d* t_{2g} state for Co^{2+} ions on *A* sites, and that the insulating gap is approximately 0.5 eV (see Fig. 5). This would imply that the tunneling current is maximal when the magnetizations of the $CoFe_2O_4$ and Fe_3O_4 layers are antiparallel and that the splitting between the spin up and spin down conduction states is ~0.13 eV. Both of these predictions are consistent with our observations.

V. CONCLUSION

In conclusion, we have successfully fabricated very thin $CoFe_2O_4/MgAl_2O_4$ bilayers on Fe_3O_4 under conditions that did not oxidize the Fe_3O_4 surface. Our investigation of the electrical and magnetic properties of these structures revealed that the $CoFe_2O_4/MgAl_2O_4$ bilayers functioned as a room temperature spin filter. In addition, we found that the current-voltage curves depended on the relative magnetic orientation of the Fe_3O_4 and $CoFe_2O_4$ layers, and that the tunneling current was maximal when the magnetizations in the two layers were antiparallel which is consistent with a partial inverse spinel structure for the $CoFe_2O_4$ layer. The net spin polarization of the electrons emitted from our junctions was calculated to have exceeded 70% for most samples. The net spin polarization emitted from the junctions and MR ratios would have been larger except for the relatively small difference in barrier heights for majority and minority spin electrons and the small value of the net spin polarization of the electrons provided by the Fe_3O_4 layer. We suggest that another insulating magnetic material with a larger difference in barrier heights will yield spin polarizations at room temperature approaching 100%. The device structure employed in this work can be extended to other ferrite materials, other half-metallic electrodes, and ferromagnetic semiconductors.

ACKNOWLEDGMENTS

M. C. acknowledges support from the Fannie and John Hertz Foundation. This work is in part supported by National Science Foundation. We are also grateful to B. Harmon and A. Yaresko for sending us some unpublished results of correlated band theory calculations for $CoFe_2O_4$.

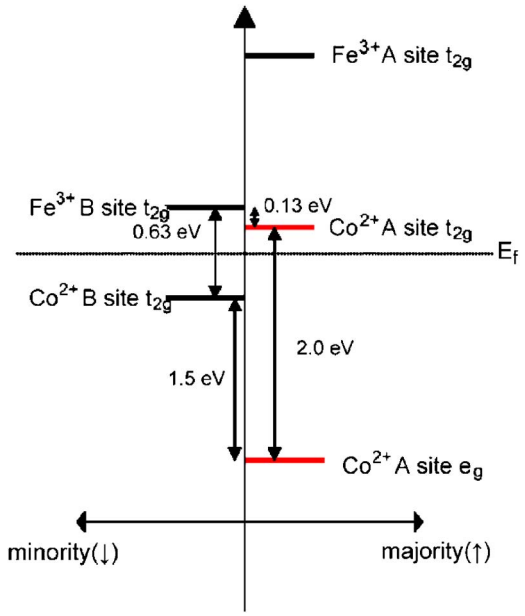

FIG. 5. (Color online) Energy level diagram for $CoFe_2O_4$ showing the majority and minority spin $3d$ states near to the Fermi level which are relevant to understanding the operation of our spin filter. The states that are present for the pure inverse spinel structure, where all the Co^{2+} ions occupy octahedral sites are shown in black, while the additional states that are present due to Co^{2+} ions occupying tetrahedral sites are shown in light gray.

APPENDIX ANALYTIC FORMULA FOR BILAYER TUNNELING CURRENT

Simmons has derived an analytic approximation for the tunneling current as a function of voltage bias for the case of a single thin layer of insulating material separating similar electrodes. This formula has proved very useful for quantifying the parameters of thin insulating tunnel barriers. However, for an insulating barrier consisting of multiple layers with very different barrier heights Simmons' formula becomes problematic because the tunneling current will be limited by the largest barrier height rather than the average barrier height. In the following we use the WKB approximation to derive an analytical formula for the tunneling current through a bilayer insulating barrier that should work as well when the barrier heights are significantly different as when they are similar. This formula can be used to determine if quantum mechanical tunneling is the dominant conduction mechanism for a particular bilayer barrier. It can also be used to extract the individual barrier heights, thicknesses, and dielectric constants of the two layers from measurements of I-V curves.

Simmons analytic formula for the tunneling current per unit area J that results when a voltage V is applied across a thin insulating barrier of thickness d separating similar electrodes can be written in the form:

$$J = J_{\text{forward}} - J_{\text{backward}}, \tag{A1}$$

where

$$J_{forward} = J_o \bar{\Phi} e^{-A\bar{\Phi}^{1/2}}, \tag{A2}$$

and

$$J_{barckward} = J_o(\bar{\Phi} + eV)e^{-A(\bar{\Phi} + eV)^{1/2}}. \tag{A3}$$

$\bar{\Phi}$ is the average barrier height with respect to the Fermi level in the electrodes and $J_o \equiv (e/\hbar)(2\pi d)^{-2}$. We will assume in the following that the electrodes are biased so that the left electrode is grounded and the right electrode is held at voltage V. Simmons derived his formula by assuming that the forward (backward) tunneling current is equal to an integral over a spherical Fermi sea of the product of the quantum mechanical tunneling probability P and the flux F_x of conduction electrons from the left (right) electrode into the barrier (i.e., in the x direction) as a function of the electron kinetic energy in the x direction E_x:

$$J = e\int_0^{E_f} P(E_x)F_x dE_x, \tag{A4}$$

where E_f is the Fermi energy in the electrodes.

The flux of electrons inside the electrodes with velocities in the x direction between v_x and $v_x + dv_x$ is $n(v_x)v_x$. Since $v_x dv_x = \frac{1}{m} dE_x$ the flux of electrons with energies between E_x and $E_x + dE_x$ is $F_x = \frac{1}{m} n(v_x) = \frac{2m^2}{(2\pi\hbar)^3} \int f(E) dv_y dv_x$, where $f(E)$ is the density of energy levels for the conduction electrons. Using the zero temperature degenerate Fermi-Dirac distribution for an ideal Fermi gas for $f(E)$ (still a reasonable approximation at room temperature) yields

$$F_x = \frac{m}{2\pi^2\hbar^3}(E_f - E_x) \tag{A4a}$$

for the flux of electrons from the left electrode into the barrier and

$$F_x = -\frac{m}{2\pi^2\hbar^3}(E_f - E_x - eV) \tag{A4b}$$

for the backward flux of electrons incident on the barrier from the right electrode. Introducing the electron kinetic energy relative to the Fermi level $\tilde{E} \equiv E_x - E_f$ we must evaluate

$$J_{forward} = -\frac{me}{2\pi^2\hbar^3}\int_{-E_f}^{0} P(\tilde{E})\tilde{E} d\tilde{E} \tag{A5a}$$

to find the forward tunneling current, and

$$J_{\text{backward}} = -\frac{me}{2\pi^2\hbar^3}\int_{-E_f}^{0} P(\tilde{E})(\tilde{E} + eV) d\tilde{E} \tag{A5b}$$

to find the backward tunneling current.

In the WKB approximation the quantum mechanical tunneling probability for a barrier of thickness d is given by

$$P = \exp\left\{-2\left(\frac{2m}{\hbar^2}\right)^{1/2}\int_0^d \sqrt{U(x) - E} dx\right\}, \tag{A6}$$

where the integral extends over the barrier and $U(x)$ is the potential energy inside the barrier. For a barrier of constant

height whose material properties are independent of position $U(x)=U_o-\mathrm{e}Vx/d$, so one might approximate the WKB tunneling probability as $P\approx e^{-A(\bar{\Phi}-\tilde{E})^{1/2}}$ where $\bar{\Phi}=U_o-\mathrm{e}V/2\text{-}E_f$ is the average barrier height above the Fermi energy and $A\equiv 2(2m/\hbar^2)^{1/2}d$. Thus in this approximation the integral we need to evaluate is

$$\int_{-E_f}^{0} e^{-A(\bar{\Phi}-\tilde{E})^{1/2}}\tilde{E}d\tilde{E}.$$

Because of the exponential dependence of the tunneling probability on barrier height, the tunneling current will be mainly determined by the value of the integrand for electron energies E_x near to the Fermi energy; i.e., for $\tilde{E}$ near to zero. Expanding the exponent about $\tilde{E}=0$ we have

$$\int_{-E_f}^{0} e^{-A(\bar{\Phi}-\tilde{E})^{1/2}}\tilde{E}d\tilde{E} \approx e^{-A\bar{\Phi}^{1/2}}\int_{-E_f}^{0} e^{A\tilde{E}/2\bar{\Phi}^{1/2}}\tilde{E}d\tilde{E} = -\frac{4\bar{\Phi}}{A^2}e^{-A\bar{\Phi}^{1/2}}. \tag{A7}$$

Substituting this expression into Eq. (A5a) yields Simmons' expression for the forward tunneling current. Simmons expression for the backward tunneling current is obtained by simply substituting $\bar{\Phi}+\mathrm{e}V$ for $\bar{\Phi}$.

In order to obtain a formula for the tunneling current in a bilayer barrier that works for arbitrary thicknesses and barrier heights for the two layers we introduce the displacement field $F\equiv V\left(\frac{\Delta x_1}{\varepsilon_1}+\frac{\Delta x_2}{\varepsilon_2}\right)^{-1}$, where Δx_1 and Δx_2 are the widths of the two layers and ε_1 and ε_2 are the dielectric constants of the layers. The potential energy inside the two layers will then be U_1-eFx/ε_1 and $U_2-eF\Delta x_1/\varepsilon_1-eF(x-\Delta x_1)/\varepsilon_2$, where $\Phi_1=U_1-E_f$ and $\Phi_2=U_2-E_f$ are the barrier heights for conduction electrons in the two layers. For a single homogeneous layer of thickness Δx the exponent of Eq. (A6) can be evaluated exactly if $U(x)-E$ is positive everywhere inside the layer:

$$\int_0^{\Delta x}\sqrt{U_0-eV_0-eFx/\varepsilon-E}dx = \frac{2\varepsilon}{3eF}\{(U_0-eV_0-E)^{3/2}-(U_0-eV_0-eF\Delta x/\varepsilon-E)^{3/2}\}, \tag{A8}$$

where V_0 is the voltage at the lef-thand side of the layer and $F\Delta x/\varepsilon$ is the voltage drop across the layer. Thus in the WKB approximation, and assuming that each layer is homogeneous, the quantum tunneling probability for each layer alone will be given by

$$P_i=\exp\left\{-\frac{2\tilde{A}}{3eV}\varepsilon_i[(U_i-eV_{i-1}-E)^{3/2}-(U_i-E-eV_i)^{3/2}]\right\}, \tag{A9}$$

where $\tilde{A}\equiv\frac{A}{d}\left(\frac{\Delta x_1}{\varepsilon_1}+\frac{\Delta x_2}{\varepsilon_2}\right)$, $V_0=0$, $V_1=F\Delta x_1/\varepsilon_1$, and $V=V_1+V_2$ is the voltage drop across the entire barrier. The overall tunneling probability will be a product of the tunneling probabilities for the two layers:

$$P=\exp\left\{-\frac{2\tilde{A}}{3eV}\sum_{i=1}^{2}\varepsilon_i[(U_i-eV_{i-1}-E)^{3/2}-(U_i-eV_i-E)^{3/2}]\right\}. \tag{A10}$$

Expressing the bracket in the exponent in Eq. (A10) in terms of $\Phi_i=U_i-E_f$ and expanding about $\tilde{E}=0$ and yields

$$[(U_i-eV_{i-1}-E)^{3/2}-(U_i-E-eV_i)^{3/2}]\cong(\Phi_i-eV_{i-1})^{3/2}-(\Phi_i-eV_i)^{3/2}-\frac{3}{2}\tilde{E}[(\Phi_i-eV_{i-1})^{1/2}-(\Phi_i-eV_i)^{1/2}].$$

Using this approximation in Eq. (A10) the generalization of Eq. (A7) becomes

$$\int_{-E_f}^{0}P(\tilde{E})\tilde{E}d\tilde{E}=\exp\left\{-\frac{2\tilde{A}}{3eV}\{\varepsilon_1[\Phi_1^{3/2}-(\Phi_1-eV_1)^{3/2}]+\varepsilon_2[(\Phi_2-eV_1)^{3/2}-(\Phi_2-eV)^{3/2}]\}\right.\int_{-E_f}^{0}\exp\left\{\frac{\tilde{A}}{eV}\{\varepsilon_1[\Phi_1^{1/2}-(\Phi_1-eV_1)^{1/2}]+\varepsilon_2[(\Phi_2-eV_1)^{1/2}-(\Phi_2-eV)^{1/2}]\}\tilde{E}\right\}\tilde{E}d\tilde{E}=-\frac{(eV)^2}{\tilde{A}^2}\{\varepsilon_1[\Phi_1-(\Phi_1-eV_1)^{1/2}]+\varepsilon_2[(\Phi_2-eV_1)^{1/2}-(\Phi_2-eV)^{1/2}]\}^{-2}\exp\left\{-\frac{2\tilde{A}}{3eV}\{\varepsilon_1[\Phi_1^{3/2}-(\Phi_1-eV_1)^{3/2}]+\varepsilon_2[(\Phi_2-eV_1)^{3/2}-(\Phi_2-eV)^{3/2}]\}\right\}. \tag{A11}$$

The expressions we obtain for J_{forward} and J_{backward} are given by

$$J_{forward}=\tilde{J}_0\frac{(eV)^2}{4}\{\varepsilon_1[\Phi_1-(\Phi_1-eV_1)^{1/2}]+\varepsilon_2[(\Phi_2-eV_1)^{1/2}-(\Phi_2-eV)^{1/2}]\}^{-2}\exp\left\{-\frac{2\tilde{A}}{3eV}\{\varepsilon_1[\Phi_1^{3/2}-(\Phi_1-eV_1)^{3/2}]+\varepsilon_2[(\Phi_2-eV_1)^{3/2}-(\Phi_2-eV)^{3/2}]\}\right\}, \tag{A12a}$$

$$J_{backward} = \tilde{J}_0 \frac{(eV)^2}{4}\{\varepsilon_1[(\Phi_1 + eV)^{1/2} - (\Phi_1 + eV_2)^{1/2}] + \varepsilon_2[(\Phi_2 + eV_2)^{1/2} - \Phi_2]\}^{-2}\exp\left\{-\frac{2\tilde{A}}{3eV}\{\varepsilon_1[(\Phi_1 + eV)^{3/2} - (\Phi_1 + eV_2)^{3/2}] + \varepsilon_2[(\Phi_2 + eV_2)^{3/2} - \Phi_2]\}\right\}, \tag{A12b}$$

where $\tilde{J}_0 \equiv \frac{e}{(2\pi)^2\hbar}\left(\frac{\Delta x_1}{\varepsilon_1} + \frac{\Delta x_2}{\varepsilon_2}\right)^{-2}$. Our final expression for the total tunneling current in a multilayer barrier will be the difference of the expressions for J_{forward} and J_{backward} given in Eq. (A12):

$$J = \tilde{J}_0 \frac{(eV)^2}{4}\left\{[\varepsilon_1(\Phi_1^{1/2} - (\Phi_1 - eV_1)^{1/2}) + \varepsilon_2((\Phi_2 - eV_1)^{1/2} - (\Phi_2 - eV)^{1/2})]^{-2}\exp\left(-\frac{2\tilde{A}}{3eV}[\varepsilon_1(\Phi_1^{3/2} - (\Phi_1 - eV_1)^{3/2}) + \varepsilon_2((\Phi_2 - eV_1)^{3/2} - (\Phi_2 - eV)^{3/2})]\right) - [\varepsilon_1((\Phi_1 + eV)^{1/2} - (\Phi_1 + eV_2)^{1/2}) + \varepsilon_2((\Phi_2 + eV_2)^{1/2} - (\Phi_2)^{1/2})]^{-2}\exp\left(-\frac{2\tilde{A}}{3eV}[\varepsilon_1((\Phi_1 + eV)^{3/2} + (\Phi_1 + eV_2)^{3/2}) + \varepsilon_2((\Phi_2 + eV_2)^{3/2} - (\Phi_2)^{3/2})]\right)\right\}, \tag{A13}$$

where $V_1 = V\frac{\Delta x_1}{\varepsilon_1}\left(\frac{\Delta x_1}{\varepsilon_1} + \frac{\Delta x_2}{\varepsilon_2}\right)^{-1}$ and $V_2 = V\frac{\Delta x_2}{\varepsilon_2}\left(\frac{\Delta x_1}{\varepsilon_1} + \frac{\Delta x_2}{\varepsilon_2}\right)^{-1}$, Δx_1 and Δx_2 are the thicknesses of the two layers, ε_1 and ε_2 are the dielectric constants in the two layers, and Φ_1 and Φ_2 are the two barrier heights. In contrast with Simmons' formula Eq. (A13) yields a tunneling current that depends on the dielectric constants in the two layers and also is asymmetric between positive and negative biases. One caveat that must be kept in mind regarding the validity of this expression is that it is only valid if $\Phi_1 > eV_1$ and $\Phi_2 > eV_1$. If either of these conditions are violated, then the terms in the sum for which this condition is violated must be modified.

[1] X. Jiang, R. Wang, R. M. Shelby, R. M. Macfarlane, S. R. Bank, J. S. Harris, and S. S. P. Parkin, Phys. Rev. Lett. **94**, 056601 (2005).
[2] D. P. DiVincenzo, J. Appl. Phys. **85**, 4785 (1999).
[3] D. Worledge and T. Geballe, J. Appl. Phys. **88**, 5277 (2000).
[4] M. Muller, W. Eckstein, and W. Heiland, Phys. Rev. Lett. **29**, 1651 (1972).
[5] E. Kisher, G. Baum, A. H. Mahan, W. Raith, and K. Schroder, Phys. Rev. Lett. **36**, 982 (1976).
[6] G. Baum, E. Kisker, A.H. Mahan, W. Raith, and B. Reihl, Appl. Phys. **14**, 149 (1977).
[7] M. Gajek, M. Bibes, A. Barthelemy, K. Bouzehouane, S. Fusil, M. Varela, J. Fontcuberta, and A. Fert, Phys. Rev. B **72**, 020406(R) (2005).
[8] M. G. Chapline and S. X. Wang, J. Appl. Phys. **97**, 123901 (2005).
[9] T. Kiyomura, M. Gomi, Y. Maruo, and H. Toyoshima, IEEE Trans. Magn. **35**, 3046 (1999).
[10] C. Kleint, M. K. Krause, R. Höhne, T. Walter, H. C. Semmelhack, M. Lorenz, and P. Esquinazi, J. Appl. Phys. **84**, 5097 (1998).
[11] L. Neel, Compt. Rend. **255**, 271 (1962)
[12] M. G. Chapline and S. X. Wang, J. Appl. Phys. **97**, 10C915 (2005).
[13] J. G. Simmons, J. Appl. Phys. **34**, 1793 (1963).
[14] D. Worledge and D. W. Abraham, Appl. Phys. Lett. **82**, 4522 (2003).
[15] V. N. Antonov, B. N. Harmon, and A. N. Yaresko, Phys. Rev. B **67**, 024417 (2003).
[16] Y. S. Dedkov, U. Rudiger, and G. Guntherodt, Phys. Rev. B **65**, 064417 (2002).
[17] G. Hu and Y. Suzuki, Phys. Rev. Lett. **89**, 276601 (2002).
[18] S. Murthy, M. Natera, J. Begum, and S. Youseef, *Proceedings of the 1st International Conference Ferrites, Tokyo* (University Park Press, 1971).
[19] G. A. Sawatzky, F. van der Woude, and A. H. Morrish, Phys. Rev. **187**, 747 (1969).
[20] G. Hu, J. H. Choi, C. B. Eom, V. G. Harris, and Y. Suzuki, Phys. Rev. B **62**, R779 (2000).
[21] T. Koide, T. Shidara, K. Ymaguchi, A. Fujimori, H. Fukutani, N. Kimizuka, and S. Kimura, J. Electron Spectrosc. Relat. Phenom. **78**, 275 (1996).
[22] K. Kim, H. Lee, M. Lee, and S. Lee, J. Appl. Phys. **91**, 9974 (2004).